Corrosion Science 136 (2018) 180–187

Contents lists available at ScienceDirect

Corrosion Science

journal homepage: www.elsevier.com/locate/corsci

The influence of temperature gradient on the corrosion of materials in molten fluorides

Yanli Wang[a,**], Chaoliu Zeng[b], Weihua Li[a,c,*]

[a] School of Chemistry and Chemical Engineering, Guangxi University, Nanning, 530004, PR China
[b] Institute of Metal Research, Chinese Academy of Sciences, Shenyang, 110016, PR China
[c] School of Chemical Engineering and Technology, Sun Yat-sen University, Zhuhai, 519082, PR China

ARTICLE INFO

Keywords:
Cr
GH3535
Molten (Li,Na,K)F
Corrosion
Temperature gradient

ABSTRACT

The corrosion of materials is a great challenge for the application of a molten salt nuclear reactor using molten fluoride salts with dissolved fissile material as fuel or using clean molten salts to cool solid nuclear fuel. Temperature gradient is one of the main driving forces. In present investigation, the corrosion of Cr and alloy GH3535 in molten (Li,Na,K)F with the temperature gradients of 600–700 and 650–700 °C is investigated. The experimental results indicate that the difference in the temperature of the melt causes the difference of the corrosion potential, and thus leads to the occurrence of galvanic corrosion. The corrosion of hot-end samples is accelerated, with a higher effectiveness for a higher temperature gradient.

1. Introduction

Molten fluoride salts have been chosen as a carrier of nuclear fuels and coolants in a Molten Salt Reactor (MSR) because of their good thermal conductivity, large specific heat, low viscosity, low vapor pressure at operating temperature, high boiling point, relatively good chemical inertness, high solubility for fission products, etc. [1]. In pure, stoichiometric salt, metal corrosion should not occur. However, in molten salt reactors with fuel dissolved in the salt, nuclear fission drives the potential in the salt to be more oxidizing, and in salt-cooled reactors using solid fuel, neutron transmutation in the salt can cause an oxidizing potential. If impurities build up in the salt, less-noble alloying elements may be dissolved into the salt [2,3]. Therefore, the corrosion of materials is an inevitable problem for the application and development of MSR. In addition, unlike conventional high temperature corrosion [4–6], most metal oxides are chemically unstable in molten fluorides and generally converted to their corresponding metal fluorides. It is reported that the main driving forces for the corrosion in molten fluorides generally involved with the impurities in fluorides and temperature gradients [7–9]. For a closed molten fluoride melt system with constant temperature, corrosion by impurities is self-limiting, that is the corrosion ceased when the impurities are expended or the solubility limits of the transition metal fluorides in the melt are reached. However, the persistent sustained corrosion occurs when temperature gradient exists in molten salt [9]. That is metals or alloys will experience continuous dissolution in hot-leg regions and re-deposition in the cold one, possibly causing structural materials failure while on service.

Over the past 60 years, large amounts of investigations on the corrosion behavior of pure metals and structural materials in molten fluorides have been conducted by many research institutions, such as ORNL, NASA, the University of Wisconsin, and National Institute for Fusion Science (NIFS) [10–14]. The weight loss of Ni-based alloys due to corrosion has been shown to increase with the increase in the Cr content. Furthermore, these studies provided the ranking order of different metals and alloys according to the corrosion resistance and formed the basic principles of alloy designing, among which the Hastelloy-N (Ni-17%Mo-7%Cr-5%Fe, mass percent) developed by ORNL exhibits a great potential for long term applications. However, there are limited reports on the temperature gradient induced corrosion behavior [15–19]. Adamson et al. [15] reported that a series of the type 316 stainless steel thermal convection loops became plugged in the cold leg due to the temperature gradient mass transfer of chromium. Koger [16] researched the compatibility of Hastelloy N with LiF-BeF_2-UF_4 melt in a low-flow temperature-gradient system (maximum temperature 704 °C, minimum temperature 538 °C). The corrosion was manifested as temperature gradient mass transfer, with a maximum weight loss of about 2.9 mg cm^{-2} at the hot leg and the largest weight gain of around 1.7 mg cm^{-2} at the colder section after 29500 h immersion. The UF_4

* Corresponding author at: School of Chemistry and Chemical Engineering, Guangxi University, Nanning, 530004, PR China and School of Chemical Engineering and Technology, Sun Yat-sen University, Zhuhai, 519082, PR China.
** Corresponding author at: School of Chemistry and Chemical Engineering, Guangxi University, Nanning, 530004, PR China.
E-mail addresses: wyl187358@gxu.edu.cn (Y. Wang), 1685680@163.com (W. Li).

https://doi.org/10.1016/j.corsci.2018.03.003
Received 14 November 2017; Received in revised form 25 February 2018; Accepted 3 March 2018
Available online 05 March 2018
0010-938X/ © 2018 Elsevier Ltd. All rights reserved.

reaction, $2UF_4 + Cr = CrF_2 + 2UF_3$, whose equilibrium is temperature dependent, provides a dissolution-re-deposition mechanism by which the alloy at high temperature is continuously depleted and the alloy at a lower temperature is continuously enriched in chromium [17]. Williams et al. [18] also observed the weight loss of the hot-end samples due to the dissolution of chromium and the weight gain of the cold-end samples due to the formation of CrF_2 in colder sections. From the limited data concerning the temperature dependence of chromium solubility obtained by ORNL, the solubility of Cr in FLiBe melt increased by 50% from 600 to 800 °C, and in molten FLiNaK by almost 150% [19]. Therefore, the differential solubility due to temperature differences can be substantial, and could drive continuous, persistent corrosion of the hot-leg alloys.

However, these above researches are mainly performed by thermogravimetric methods to study the effect of temperature gradients, by which the corrosion processes cannot be examined in situ. In actual, the corrosion of materials in molten fluorides with temperature gradients occurs by a galvanic corrosion mechanism. The hot-leg section is the anode of the corrosion battery and the cold-leg part is the cathode. Therefore, electrochemical methods for galvanic corrosion can be employed to study the corrosion of materials in molten fluorides with thermal gradients in-situ. These electrochemical techniques have been proved effective in understanding the corrosion mechanism and kinetics, with more information obtained for the corrosion processes. There have been some reports on the electrochemical investigation of corrosion in molten fluorides [20–24]. But this has not been done extensively in molten fluorides.

In present study, the corrosion behavior of metal Cr and superalloy GH3535 is investigated in molten (Li,Na,K)F with temperature gradients by electrochemical and thermogravimetric methods in an attempt to understand the dissolution-re-deposition reactions in depth.

2. Experimental procedures

A ternary eutectic mixture of 46.5LiF-11.5NaF-42KF (mole percent) was used in the present study. The salt was produced and provided by Shanghai Institute of Applied Physics, CAS. The salt was purified through sparging with argon H_2/HF followed by H_2. The impurities of the salt are as follows: 14 ppm Fe, 74 ppm Ni, 6 ppm Cr, 11 ppm Ca, 19 ppm Mg, 8 ppm Zn, 10 ppm P, and the other elements are below the quantitative detection limits of Inductively Coupled Plasma Optical Emission Spectrometer (ICP-OES). A mixture of (Li,Na,K)F was put into a graphite crucible (supplied by Sinosteel Shanghai Advanced Graphite Materials Company, China). The salt mixture was further dried at 200 °C in the reaction chamber under vacuum, and then under the protection of Ar (99.9993% purity) for 20 h before the furnace was heated to the experimental temperatures.

The materials used in the present study are pure metal Cr (99.19 wt.% purity) and a hot rolled Ni-based superalloy GH3535 (supplied by Institute of Metal Research, Chinese Academy of Sciences). The chemical composition and microstructure of GH3535 are already given in ref. [20]. The bulk materials were cut into specimens with a size of 5 mm × 30 mm × 2 mm by an electric spark cutting machine, followed by grinding down to 1000 grit SiC paper, cleaning with distilled water and then drying. A Pt wire (99.95 wt.% purity, supplied by Shenyang Gold of College, China) was spot welded to one end of the pure Cr specimens and a GH3535 wire was spot welded to one end of the GH3535 specimens for electrical connection. The sample was sealed in an alumina tube (99.9 wt.% purity) with high-temperature cement (supplied by Hubei Huitian Adhensive Enterprise Co., Ltd), with a length of 15 mm exposed. The cement was dried at room temperature for 24 h and then further solidified at 300 °C for 2 h. The exposed surfaces of samples were polished again with 1000 grit SiC paper, rinsed, and dried before tests. In order to study the temperature gradient induced corrosion behavior, galvanic corrosion measurements, with a Pt electrode (99.95 wt.% purity, supplied by Shenyang Gold of College, China) as the reference electrode, were conducted in a closed Hastelloy C276 alloy (Ni-16Cr-17Mo-4W, wt.%) chamber under the protection of non-flowing high-purity argon by coupling the two same samples at the hot and cold legs electrically, as shown in Fig. 1. Two temperature gradients, i.e. 600–650 and 600–700 °C were selected. When the melt is heated to the target temperatures, we calibrated the temperature every time before the experiment at each end of the cell to ensure the working area is in the target temperatures. The two couples used in the galvanic corrosion tests were the Cr (the hot-leg section) – Cr (the cold-leg section) couple and the GH3535 (the hot-leg section) – GH3535 (the cold-leg section) couple. The galvanic potential (E_g) and current (I_g) of the Cr and GH3535 couples were simultaneously recorded.

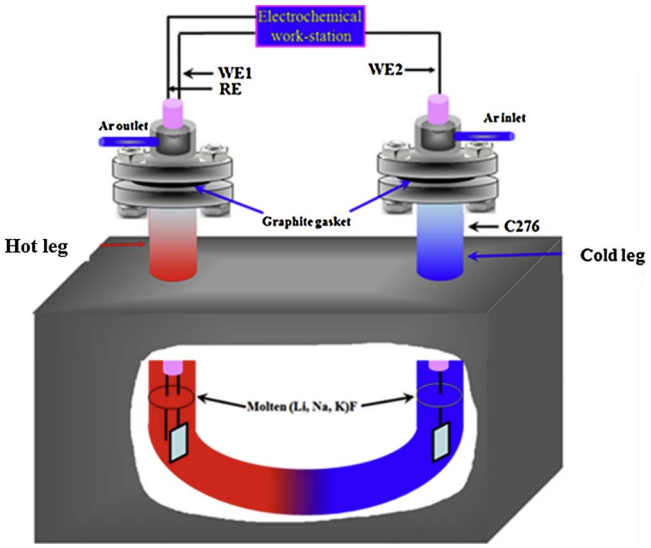

Fig. 1. A schematic diagram for temperature-gradient induced molten salt corrosion.

Electrochemical tests at isothermal conditions including the open circuit potential and potentiodynamic polarization were conducted with a Princeton Applied Research PARSTAT 2273 potentiostat/Galvanostat system in a closed stainless steel chamber under the protection of non-flowing high-purity Ar, as reported in Ref. [21]. A conventional three-electrode system with a Pt electrode as the reference electrode and a graphite plate (supplied by Sinosteel Shanghai Advanced Graphite Materials Company, China) as the counter electrode was used. Potentiodynamic polarization was undertaken at a scan rate of 20 mV min^{-1}.

After galvanic corrosion, the corroded samples covered with the remaining salts were mounted in epoxy resin and then their metallurgical sections were prepared using kerosene as coolant for grinding and polishing, with an attempt to examine the corroded metal/salt interface. Scanning electron microscope (SEM) coupled with an energy dispersive X-ray microanalysis (EDX) was used to characterize the corroded metals.

In addition to electrochemical measurements, immersion tests for 24 h were also conducted to obtain mass changes of the galvanic couples at different temperature gradients. The two same samples at the hot and cold legs coupled electrically were suspended in the melt by a Pt wire for Cr couples and a GH3535 wire for the GH3535 couples. After experiments, the samples were taken out of the melt, cooled down to room temperature, and finally cleaned in distilled water to remove the residual salts. All of the samples were weighed by a balance with an accuracy of 10^{-5} g.

3. Results and discussion

3.1. Free corrosion potential measurements

Fig. 2 presents the relationship between the potential differences

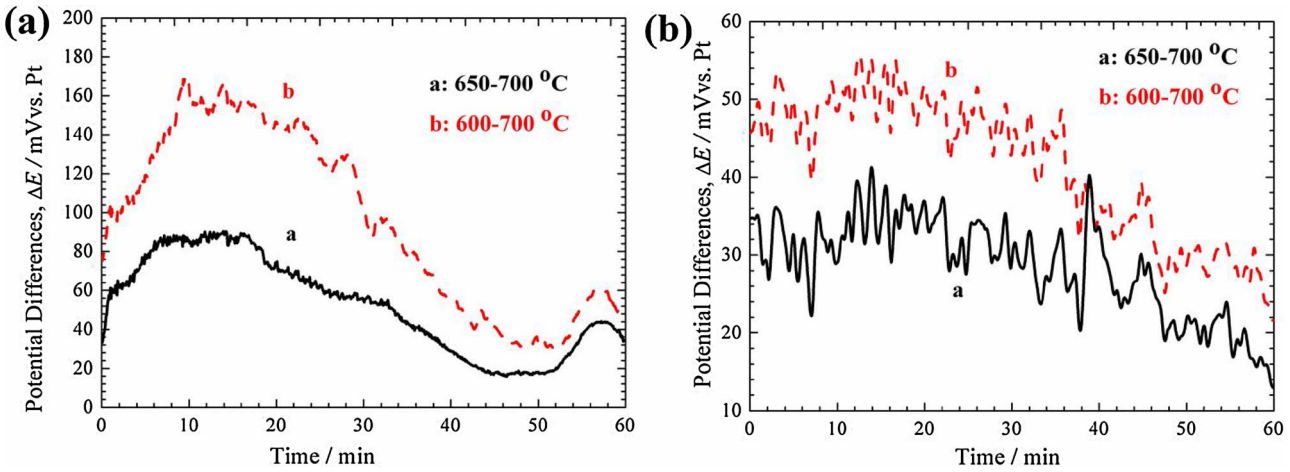

Fig. 2. Potential differences curves of Cr (a) and GH3535 (b) in molten (Li,Na,K)F at different temperatures under Ar environment.

and exposure time for pure metal Cr and GH3535 in molten (Li,Na,K)F at the temperature of 650–700 and 600–700 °C, respectively. The results indicate that the potential difference ΔE for Cr and GH3535 becomes bigger with the temperature difference increasing. ΔE for Cr at 650–700 °C moves positively in the initial 10 min, and then decreases to about 20 mV, and finally increases to about 30 mV ΔE for Cr at 600–700 °C shows the same change, with a final value of about 50 mV. After 1 h immersion, ΔE for GH3535 at the temperature of 650–700 and 600–700 °C is around 15 and 25 mV, respectively, with a significant fluctuation. Therefore, it will be concluded that the difference in the temperature of the melt causes the difference of the corrosion potential of metals, and thus probably leads to the galvanic corrosion.

3.2. Potentiodynamic polarization measurements

The potentiodynamic polarization curves of Cr and GH3535 in molten (Li,Na,K)F at 600, 650 and 700 °C are shown in Fig. 3. The results reveal that both Cr and GH3535 are in active states at the corrosion potential. Furthermore, the anodic reaction current densities of Cr and GH3535 increase significantly with the increasing temperature while the cathodic reaction current densities of Cr and GH3535 change little. Due to the fact that the corrosion process of Cr and GH3535 has only a kinetic time constant and is not controlled by the diffusion of ions obtained from the impedances of Cr [21] and GH3535 [20] in pure molten (Li,Na,K)F at 700 °C, the Tafel extrapolation method [25] is used to get the kinetic parameters of pure metal Cr and GH3535 in molten (Li,Na,K)F at 600, 650 and 700 °C and the results are shown in Tables 1 and 2, respectively. The paremeters, b_a and b_c, are the slope in anodic region and slope in cathodic region of Fig. 3, respectively. It can be seen that the corrosion current densities, I_{corr}, of Cr at 600, 650 and 700 °C are calculated to be about 375, 382 and 415 μA cm^{-2}. I_{corr} for GH3535 increases from 82 μA cm^{-2} for 600 °C to 98 μA cm^{-2} for 700 °C. The above results suggest that the temperature increasing can significantly accelerate the corrosion of Cr and GH3535 in the melt (Table 2).

Table 1
Electrochemical parameters obtained by Tafel linear fitting of polarization curves for Cr in molten (Li,Na,K)F at different temperatures.

T (°C)	b_a (mV dec^{-1})	b_c (mV dec^{-1})	E_{corr} (mV vs. Pt)	I_{corr} (μA cm^{-2})
600	111	−135	−467	375
650.	75.5	−167.4	−489	382
700	80.5	−155.3	−508	415

Table 2
Electrochemical parameters obtained by Tafel linear fitting of polarization curves for GH3535 in molten (Li,Na,K)F at different temperatures.

T (°C)	b_a (mV dec^{-1})	b_c (mV dec^{-1})	E_{corr} (mV vs. Pt)	I_{corr} (μA cm^{-2})
600	153.9	−96.5	−218	82
650	135	−89	−230	89
700	93.9	−78.1	−240	98

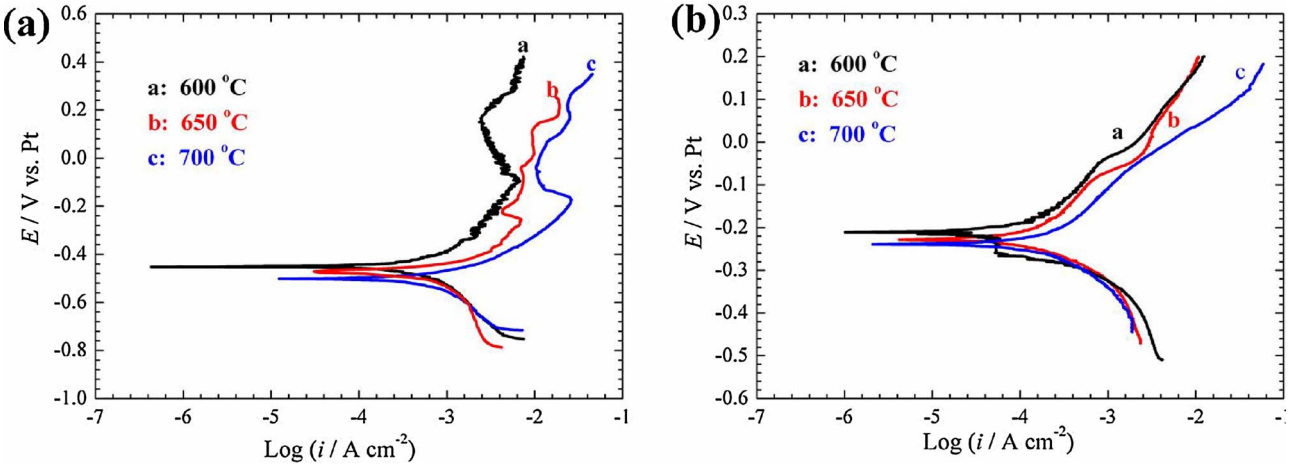

Fig. 3. Potentiodynamic polarization curves of Cr (a) and GH3535 (b) at different temperatures in molten (Li,Na,K)F under Ar environment.

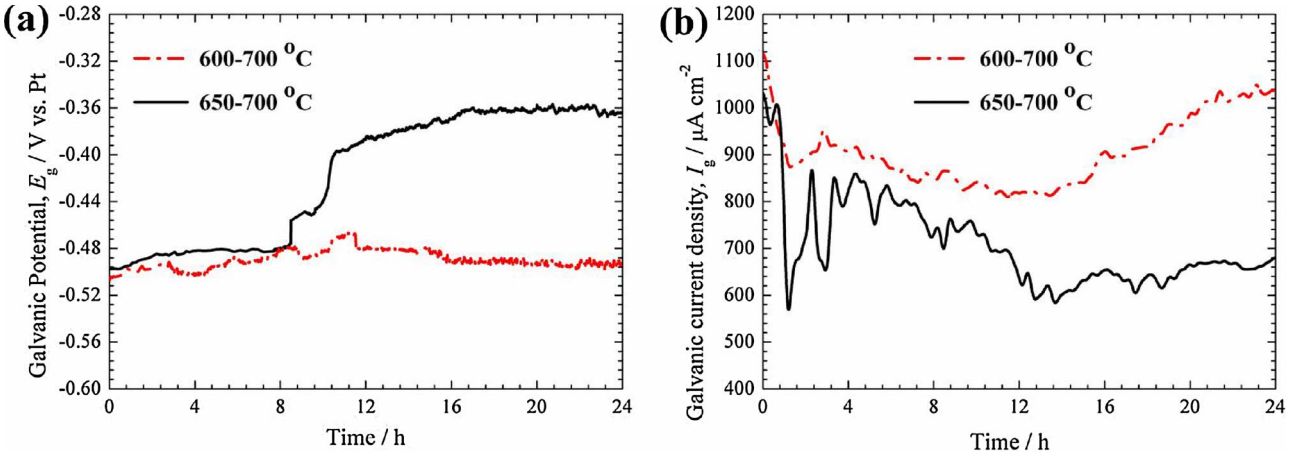

Fig. 4. Time dependence of the galvanic potential (a) and galvanic current density (b) for Cr in molten (Li,Na,K)F with the temperature gradients of 650–700 °C and 600–700 °C.

3.3. Galvanic corrosion measurements

Fig. 4 gives the time dependence of the galvanic potential and galvanic current density for Cr in molten (Li,Na,K)F with the temperature of 650–700 and 600–700 °C. Based on the above free corrosion potential results, it can be inferred that Cr at 700 °C in molten (Li,Na,K)F with the temperature gradients of 650–700 and 600–700 °C is the anode during the galvanic corrosion process. E_g for the Cr couple at the temperature gradient of 650–700 °C keeps at around −480 mV vs. Pt during the initial 8 h, and then increases drastically to around −380 mV vs. Pt and levels off, which may be due to a steady state amount of Cr dissolved in the melt after about 12 h. E_g for the Cr couple at the temperature gradient of 600–700 °C are about −500 mV vs. Pt, with a small fluctuation during the experimental duration of 24 h I_g for the Cr couple at the temperature gradient of 650–700 °C decreases drastically during the initial 2 h, and then goes through obvious fluctuation, finally keeps at around 650 μA cm^{-2}. I_g for the Cr couple at the temperature gradient of 600–700 °C decreases obviously from around 1100 to 860 μA cm^{-2} after immersion in the melt for about 2 h, followed by slight decrease, and then increases slowly again to about 1000 μA cm^{-2}.

Fig. 5 shows the change of galvanic potential and galvanic current density with exposure time for GH3535 in molten (Li,Na,K)F with the temperature gradients of 650–700 and 600–700 °C. Similarly, GH3535 at 700 °C for the two GH3535 couples at the temperature gradients of 650–700 and 600–700 °C are the anode during the galvanic corrosion process. E_g for the GH3535 couple at the temperature gradient of 650–700 °C increases slowly from about −210 to −190 mV vs. Pt during the initial 12 h, and then goes through a drastic fluctuation. E_g for the GH3535 couple at the temperature gradient of 600–700 °C shows a slow increase in the initial stage, followed by obvious fluctuations. I_g for the GH3535 couple at the temperature gradient of 650–700 °C is around 345 μA cm^{-2} and changes little with immersion time. I_g for the GH3535 couple at the temperature gradient of 600–700 °C shifts positively to about 420 μA cm^{-2} during the experimental duration of 24 h, with some fluctuations.

From the above results, we conclude that the fluctuation of the galvanic potentials and galvanic current densities for Cr and GH3535 couples may be related to the dissolution and re-deposition reactions on the surfaces of the couples. Furthermore, the container material Hastelloy C276 also corroded in the melt, resulting in the presence of the impurities of Fe^{2+}, Fe^{3+} and Mo^{2+} in the melt. These impurities could be consumed in corrosion (for example $FeF_2 + Cr = CrF_2 + Fe$), causing a fluctuation. For the GH3535 couples, after Cr at the surface has been oxidized, the rate of Cr oxidation reaction becomes limited by the grain boundary diffusion of Cr in GH3535 [26,27]. Furthermore, the galvanic current density increases with the increasing of the temperature gradient.

3.4. Characterization of the galvanically corroded samples

After galvanic corrosion, severe corrosion is observed for the anodic metals, whose thickness is significantly decreased. To examine the corroded metal/salt mixture interface, the cross sections of the corroded samples covered with the remaining salts were prepared for SEM observations. Figs. 6 and 7 present the cross-sectional morphologies of

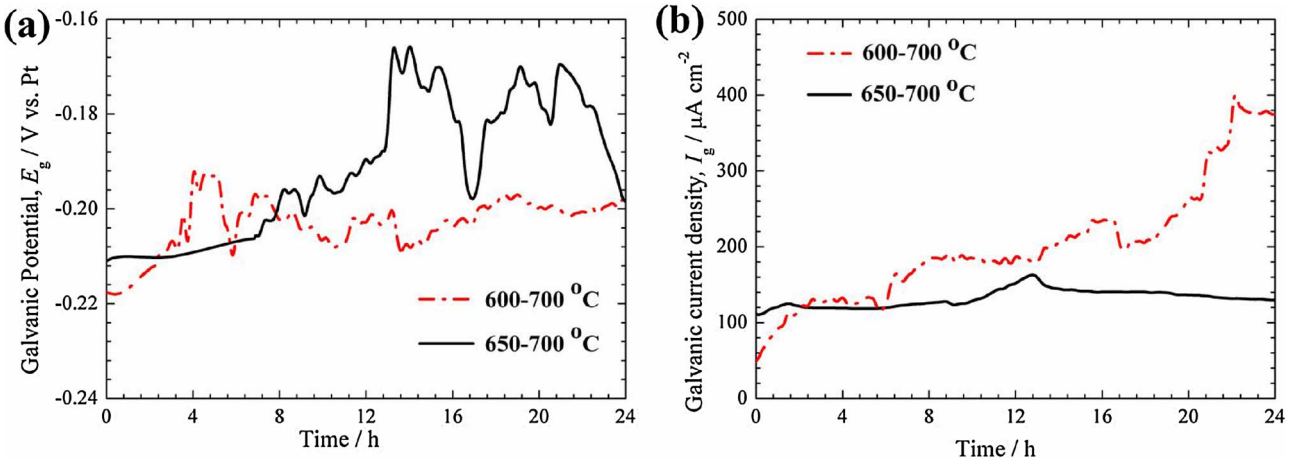

Fig. 5. Time dependence of the galvanic potential (a) and galvanic current density (b) for GH3535 in molten (Li,Na,K)F with the temperature gradients of 650–700 °C and 600–700 °C.

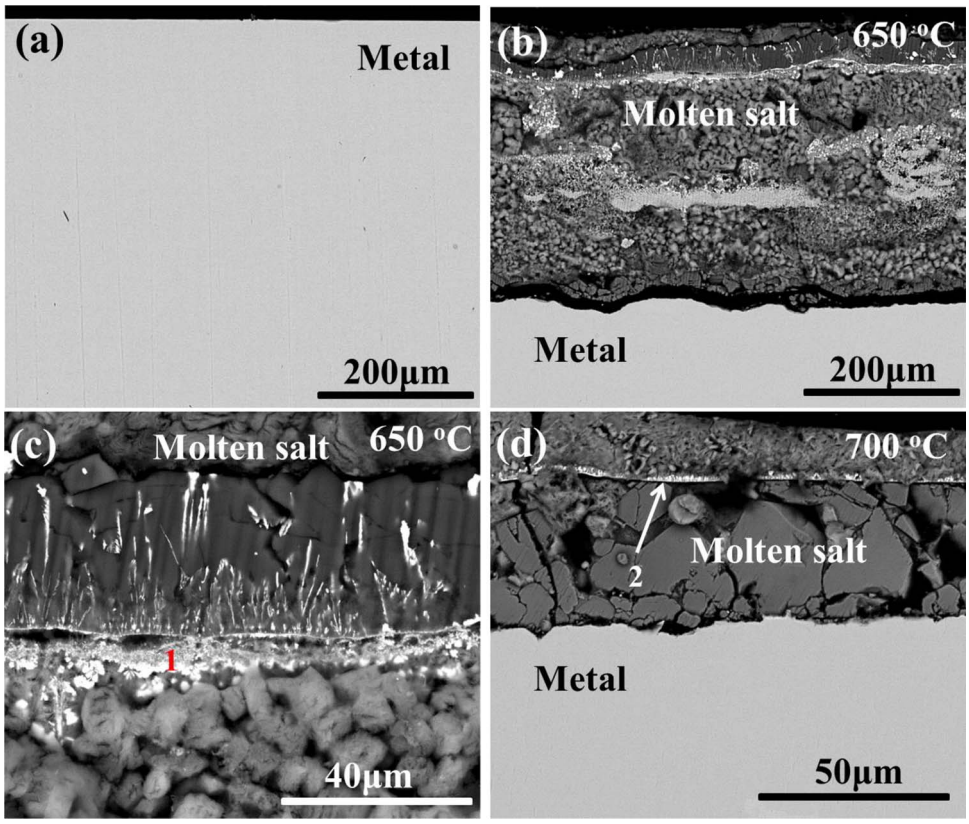

Fig. 6. Cross-sectional morphologies of pure Cr before and after galvanic corrosion in molten (Li,Na,K)F with the temperature gradient of 650–700 °C for 24 h: (a) before corrosion, (b, c) 650 °C after corrosion, (d) 700 °C after corrosion.

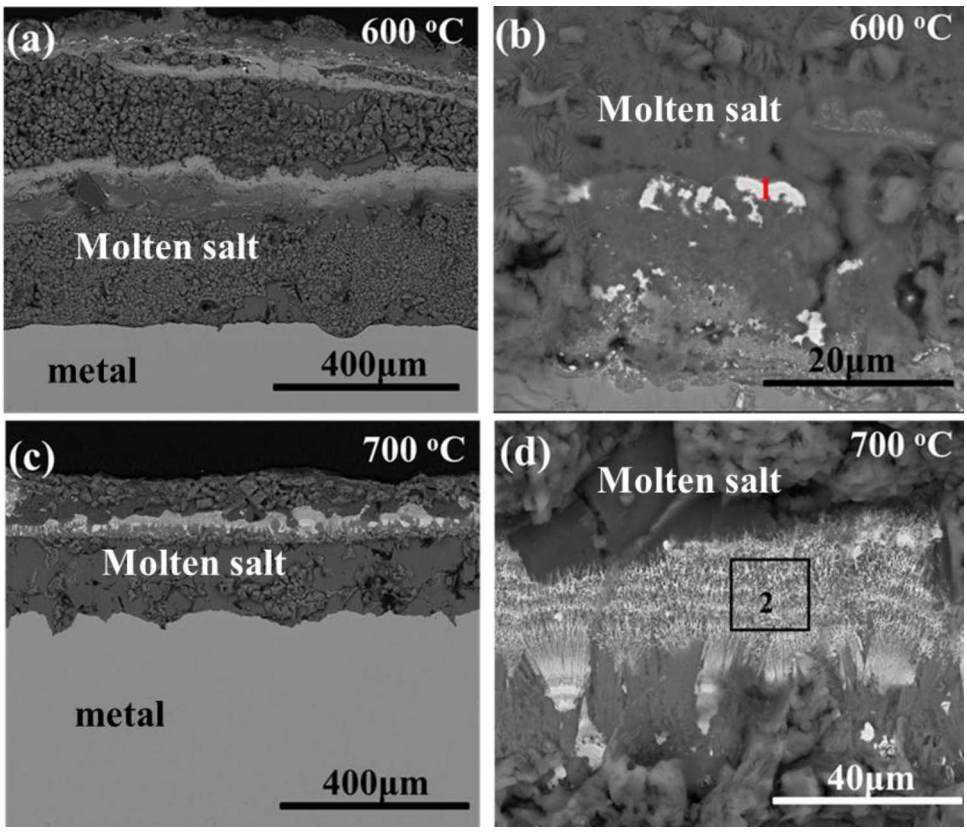

Fig. 7. Cross-sectional morphologies of pure Cr after galvanic corrosion in molten (Li,Na,K)F with the temperature gradient of 600 (a, b) −700 °C (c, d) for 24 h.

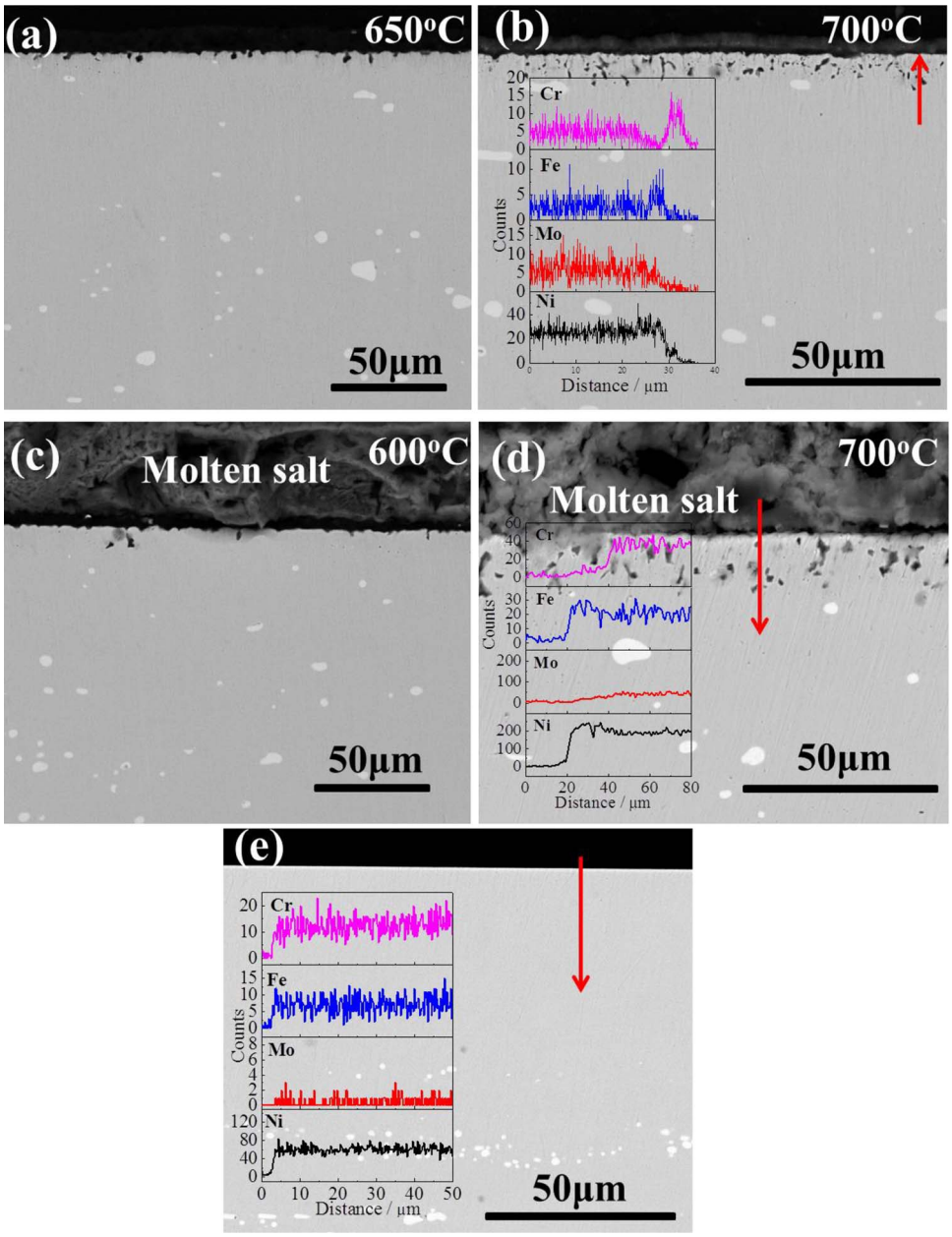

Fig. 8. Cross-sectional morphologies of GH3535 after galvanic corrosion in molten (Li,Na,K)F with the temperature gradients of 650 (a) −700 °C (b) and 600 (c) −700 °C (d) for 24 h and before galvanic corrosion (e).

the Cr couples before and after galvanic corrosion in molten (Li,Na,K)F with the temperature gradients of 650–700 and 600–700 °C for 24 h. It can be seen that compared with the sample before galvanic corrosion (Fig. 6a), both the hot-leg and cold-leg Cr samples are severely corroded through the non-uniform dissolution into the melt. For the Cr couple at the temperature gradient of 650–700 °C, some Mo/Fe-containing products, with a chemical composition of 15.89Mo-9.96Cr-6.54Fe-57.27O-10.24 K (at.%) for the point 1 in Fig. 6b, are observed on the surface of the cathode Cr, And some Mo-containing products are observed on the surface of the anode Cr, with a chemical composition of 16.18Mo-14.94Cr-47.10O-4.66K-17.12F (at.%) for the point 2 of Fig. 6c. For the Cr couple in molten (Li,Na,K)F with the temperature gradient of 600–700 °C, some Mo/Fe-containing products are observed on the surface of the anode and cathode Cr, with a chemical composition of 47.94Mo-3.32Cr-16.89Fe-30.25O-1.60 K (at.%) for the point 1 of Fig. 7b and a chemical composition of 14.59Mo-19.03Cr-2.04Fe-63.18O-1.16 K (at.%) for the zone of Fig. 7d.

Fig. 8 shows the cross-sectional morphologies of GH3535 before and after galvanic corrosion in molten (Li,Na,K)F with the temperature gradients of 650–700 and 600–700 °C for 24 h. Compared with the sample before galvanic corrosion (Fig. 8e), the GH3535 couples at both temperature gradients suffer from non-uniform dissolution, while the hot-leg GH3535 is more severely corroded than the cold-section GH3535. For the GH3535 couple in molten (Li,Na,K)F with the temperature gradient of 650–700 °C, the corrosion of the anode GH3535 occurs mainly through the preferential dissolution of Cr from the substrate alloy, forming a Cr-depleted zone with a depth of around 8 μm (Fig. 8b). However, a Mo/Cr-depleted layer with a depth of about 15 μm is observed (Fig. 8d) for the corrosion of the anode GH3535 of the couple in molten (Li,Na,K)F with the temperature gradient of 600–700 °C. No Mo/Cr-depleted zone is observed before the galvanic corrosion (Fig. 8a). Furthermore, large amounts of internal voids are formed in the corrosion layers of GH3535 samples in molten (Li,Na,K)F with the temperature gradients of 650–700 and 600–700 °C, which is

Table 3
Mass loss of pure Cr and GH3535 after immersion in molten (Li,Na,K)F with the temperature gradients of 650–700 °C and 600–700 °C for 24 h.

Samples	650–700 °C (mg cm^{-2})		600–700 °C (mg cm^{-2})	
	650	700	600	700
Cr	84	141	57	162
GH3535	1.23	2.17	0.91	2.89

mainly related to the aggregation of vacancies left by the outward diffusion of Cr and Mo. Furthermore, the voids observed in Fig. 8 are consistent with similar voids observed in Hastelloy-N by Koger [28].

3.5. Mass loss of the galvanic couples

In order to further research the corrosion behavior of metals and alloys in the temperature gradient molten salt system, the mass loss of Cr and GH3535 couples after immersion in molten (Li,Na,K)F with the temperature gradients of 650–700 and 600–700 °C for 24 h is investigated, as shown in Table 3. When the temperature gradient difference is 100 °C, the mass loss for the anode Cr is about 162 mg cm^{-2}, which is larger than that for the anode Cr at the temperature difference of 50 °C. Compared to Cr, the mass loss of anode GH3535 is much smaller, with the values of about 2.89 and 2.17 mg cm^{-2} at the temperature gradients of 600–700 and 650–700 °C, respectively. Apparently, the larger the temperature gradient is, the more severe corrosion the hot-leg samples experience. However, the mass gain of the cold-leg samples is not observed in our experiment. It is possible that in the cold section, mass was deposited on the tube and not on the samples.

3.6. Discussion

The above results show clearly that the temperature difference causes the difference corrosion potential of the metals in the melt, which leads to significant galvanic corrosion.

The average values of E_g and I_g are calculated by integral method, as shown in Tables 4 and 5. According to the relationship between the anodic dissolution current density (I_a) and galvanic current density (I_g) [22] and the experimental results of the galvanic corrosion, the galvanic effects (γ) are calculated and listed in Tables 4 and 5. It is seen that all of the values of γ are larger than 1, suggesting that the corrosion of the anode samples at the hot leg is accelerated, with a higher effectiveness for a higher temperature gradient.

According to the thermodynamic data from HSC Chemistry version 6.0 database [29], the standard Gibbs energy $\Delta G^{\circ}_{Me/Mey+}$ of different fluorides at different temperatures is calculated, as listed in Table 6. This indicates that the free energy of salt constituents such as LiF, NaF, and KF, is more negative than that of the fluorides for any constituents of samples, thus corrosion of samples can hardly occur in pure molten fluoride salts at 600, 650 and 700 °C. In our closed experimental environment, alumina was used in the system, porosity in alumina could allow moisture ingress into the experiment. And the Ar may also contain several ppm moistures. Therefore, a certain amount of the impurity H_2O inevitably exists, and the corrosion induced by dissolved water

Table 4
Glavanic corrosion parameters of Cr in molten (Li,Na,K)F with the temperature gradients of 650–700 °C and 600–700 °C.

Couples	(μA cm^{-2})	(mV vs. Pt)	E_{corr} (mV vs. Pt)	I_a (μA cm^{-2})	I_{corr} (μA cm^{-2})	γ
650–700 °C	705	−417	−515	719	415	1.73
600–700 °C	905	−489	−515	1330	415	3.21

Table 5
Glavanic corrosion parameters of GH3535 in molten (Li,Na,K)F with the temperature gradients of 650–700 °C and 600–700 °C.

Couples	(μA cm^{-2})	(mV vs. Pt)	E_{corr} (mV vs. Pt)	I_a (μA cm^{-2})	I_{corr} (μA cm^{-2})	γ
650–700 °C	132	−191	−235	145	98	1.10
600–700 °C	201	−203	−235	245	98	1.22

Table 6
Standard Gibbs energy $\Delta G^{\circ}_{Me/Mey+}$ of different metal fluorides at different temperatures.

Elements	Most stable fluorides	$\Delta G^{\circ}_{Me/Mey}$ (kJ mol^{-1})		
		600 °C	650 °C	700 °C
Cr	CrF_2	−210.40	−211.22	−211.98
Fe	FeF_2	−131.00	−131.54	−131.98
Ni	NiF_2	−65.77	−65.09	−64.33
Mo	MoF_2	−160.22	−163.16	−166.14
Li	LiF	−304.90	−303.52	−302.13
Na	NaF	−257.95	−256.22	−254.47
K	KF	−251.97	−250.41	−248.84

ceased when the H_2O has been consumed. However, when the temperature gradient exists in molten (Li,Na,K)F, the corrosion will continue. Due to the fact that samples exhibit different potentials in molten (Li,Na,K)F with different temperatures, the accelerated corrosion for the hot-end samples and inhibited corrosion for the cold-end samples occurs when they are in electrical contact. For the Cr containing alloy, Cr diffuses outward from the alloy to react with the dissolved HF, which is produced by the reaction of H_2O and fluorides, to form CrF_2 which is then dissolved in the melt. Then, the generated Cr^{2+} at the high temperature diffuses to be reduced to metal Cr and precipitates on the surface of the cold-leg alloy. The whole corrosion processes are illustrated in Fig. 9. Obviously, a negative gradient for the equilibrium concentration of CrF_2 exists on the surface of the alloy/melt from hot-leg samples to the colder-leg samples, i.e.

$$\left(\frac{d[\text{Equilibrium concentration}_{(CrF_2)}]}{dx}\right)_{x=0} < 0 \quad (1)$$

The reduction of Cr^{2+} on the surface of the cold-leg samples results in the continuously dissolution of the hot-leg alloys. The corrosion mechanism is similar to the Rapp-Goto criterion of the hot corrosion [30]. Differently, the dissolution and re-deposition reactions are the anodic and cathodic electrochemical reactions of a corrosion battery, and Cr is mainly deposited on the surface of the alloy, not in the melt. The outward diffusion of Cr can leave some vacancies in the substrate which can then aggregate to form internal voids. Due to fact that the material of the experimental system (Fig. 1) is Hastelloy C276, some metal ions, such as Cr, Fe, Mo, Ni, may exist in the melt. Therefore, some ions may be partially reduced and deposited on the surfaces of alloys or metals by the disproportionate reactions during the corrosion tests, such as the precipitation of Mo observed in Figs. 6 and 7. Furthermore, the Fe, Mo, Ni fluorides would all be capable of oxidizing Cr to CrF_2. This could be another source of impurities in the melt which promote Cr oxidation.

In the GH3535 couples, after Cr at the surface of the metal has been oxidized, the rate of Cr oxidation will become limited by Cr grain boundary diffusion in GH3535 [26,27]. The reaction rate of the Cr couple would be closer to a pure chemical kinetic reaction rate since the metal is pure Cr. The rate of the temperature-gradient induced galvanic corrosion is also closely related to the oxidation/reduction potential, the diffusion rate of particles in melt, materials, reaction time and so on. From the above results of the mass loss for Cr and GH3535, the existence of temperature gradient in the melt accelerates the corrosion

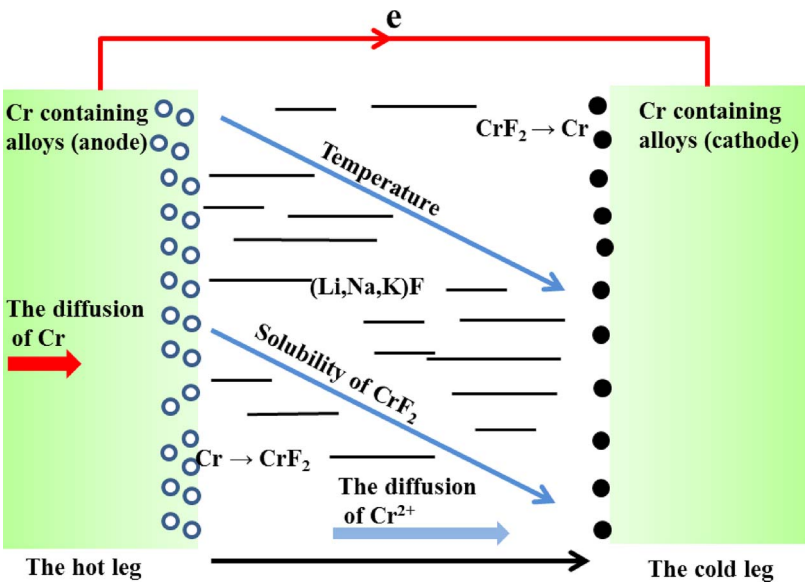

Fig. 9. A schematic diagram for the corrosion of alloys in molten (Li,Na,K)F with existence of thermal gradients.

rate of the hot-leg Cr and GH3535, while no mass gain is observed for the cold-end samples, which may be related to the limited inhibition degree of the dissolution reactions and the shorten immersion time. The mechanism is still needed to be further researched (Table 5).

4. Conclusions

The corrosion potentials for Cr and GH3535 shift negatively, while the corrosion current densities increases with the molten (Li,Na,K)F temperature increasing from 600 to 700 °C. In addition, both of Cr and GH3535 will suffer from galvanic corrosion when the two same samples are in electrical contact in molten (Li,Na,K)F where temperature gradients exist. The galvanic effects of all the couples are larger than 1. The samples at the high temperature sections act as the anodes during the galvanic corrosion process, and their dissolution is accelerated greatly, with a higher effectiveness for a higher temperature gradient. The dissolved metal ions diffuse to be reduced on the cold-section samples, resulting in the continued dissolution of the hot-end samples.

In the future, a lot of works need to be done. More materials such as Mo, Ni and Hastelloy N, 316L should be tried in the temperature-gradient system. A new natural circulation loop should be used to repeat all the experiments. Bubbling H_2 through the (Li,Na,K)F melt may be used to fix the salt redox potential.

Acknowledgements

This project is supported by the Bagui scholars program of Guangxi autonomous region in 2016, the Academician Workstation Building Project of Guangxi Zhuang Autonomous Region Scientific and Technological Department [Grant No. [2014] 91], and National Natural Science Foundation of China [Grant Nos. 51271190 and 51525903].

References

[1] D.F. Williams, Assessment of Candidate Molten Salt Coolant for the NGNP/NHI Heat Transfer Loop, ORNL/TM-2006/69, (2006).
[2] L.M. Toth, G.D.D. Cul, S. Dai, D.H. Metcalf, Molten fluoride fuel salt chemistry, AIP Conf. Proc. 346 (1995) 617–626.
[3] Paul N. Haubenreich, J.R. Engel, Experience with the molten-salt reactor experiment, Nucl. Appl. Technol. 8 (1970) 118–136.
[4] H. Zhu, R. Holmes, T. Hanley, J. Davis, K. Short, L. Edwards, High-Temperature corrosion of helium ion-irradiated Ni-based alloy in fluoride molten salt, Corros. Sci. 91 (2015) 1–6.
[5] A. Pfennig, B. Fedelich, Oxidation of single crystal PWA 1483 at 950°C in flowing air, Corros. Sci. 50 (2008) 2484–2492.
[6] M. Hofmeister, L. Klein, H. Miran, R. Rettig, S. Virtanen, R.F. Singer, Corrosion behaviour of stainless steels and a single crystal superalloy in a ternary LiCl-KCl-CsCl molten salt, Corros. Sci. 90 (2015) 46–53.
[7] J.H. Devan, Effect of Alloying Additions on Corrsion Behavior of Nickel-molybdenum Alloys in Fused Fluorine Mixtures, ORNL-TM-2021, (1969).
[8] L.C. Olson, J.W. Ambrosek, K. Sridharan, M.H. Anderson, T.R. Allen, Materials corrosion in molten LiF-NaF-KF salt, J. Fluorine Chem. 130 (2009) 67–73.
[9] M.S. Sohal, M.A. Ebner, P. Sabharwall, P. Sharpe, Engineering Database of Liquid Salt Thermophysical and Thermochemical Properties, INL/EXT-10-18297, (2010).
[10] D. Williams, L. Toth, K. Clarno, Assessment of Candidate Molten Salt Coolants for the Advanced High Temperature Reactor (AHTR), ORNL/TM-2006/12, (2006).
[11] M.W. Rosenthal, P.N. Haubenreich, R.B. Briggs, The Development Status of Molten Salt Breeder Reactors, ORNL-4812, (1972).
[12] Luke Olson, Kumar Sridharan, Mark Anderson, Todd Allen, Intergranular corrosion of high temperature alloys in molten fluoride salts, Mater. High Temp. 27 (2014) 145–149.
[13] Y.L. Wang, Q. Wang, H.J. Liu, C.L. Zeng, Effect of grain refinement on the corrosion of Ni-Cr alloys in molten (Li,Na,K)F, Corros. Sci. 109 (2016) 43–49.
[14] W. Xue, X. Yang, J. Qiu, H. Liu, B. Zhao, H. Xia, X. Zhou, P. Huai, H. Liu, J. Wang, Effects of Cr^{3+} on the corrosion of SiC in LiF-NaF-KF molten salt, Corros. Sci. 114 (2017) 96–101.
[15] G.M. Adamson, R.S. Crouse, W.D. Manly, Interim Report on Corrosion by Alkali Metal Fluorides, ORNL-2337, (1959).
[16] J.W. Koger, Effect of FeF_2 Addition on Mass Transfer in a Hastelloy N-LiF-Be F_2-UF_4 Thermal Convection Loop System, ORNL-TM-4188, (1972), pp. 1–19.
[17] B.J. You, Study on Corrosion Behavior of Nickel- Based Alloys in FLiNaK Molten Salt, National Tsing Hua University, 2010.
[18] D.F. Williams, D.F. Wilson, L.M. Toth, J. Caja, J.R. Keiser, Research on molten fluorides as high temperature heat transfer agents, American Nuclear Society Winter Meeting (2003) 1–12.
[19] D. Williams, L. Toth, K. Clarno, Assessment of Candidate Molten Salt Coolants for the Advanced High Temperature Reactor (AHTR), Department of Energy, 2006.
[20] Y. Wang, H. Liu, G. Yu, J. Hou, C. Zeng, Electrochemical study of the corrosion of a Ni-based alloy GH3535 in molten (Li,Na,K)F at 700°C, J. Fluorine Chem. 178 (2015) 14–22.
[21] Y.L. Wang, Q. Wang, H.J. Liu, C.L. Zeng, Effects of the oxidants H_2O and CrF_3 on the corrosion of pure metals in molten (Li,Na,K)F, Corros. Sci. 103 (2016) 268–282.
[22] Y. Wang, H. Liu, C. Zeng, Galvanic corrosion of pure metals in molten fluorides, J. Fluorine Chem. 165 (2014) 1–6.
[23] B.B. El-Dasher, J. Farmer, J. Ferreira, M.S. de Caro, A. Rubenchik, A. Kimura, Corrosion of oxide dispersion strengthened iron-chromium steels and tantalum in fluoride salt coolant: an in situ compatibility study for fusion and fusion-fission hybrid reactor concepts, J. Nucl. Mater. 419 (2011) 15–23.
[24] D. Ludwig, L. Olson, K. Sridharan, M. Anderson, T. Allen, High temperature electrochemistry of molten fluoride salt for measurement of dissolved chromium, Corros. Eng. Sci. Technol. 46 (2011) 360–364.
[25] S. Fabre, C. Cabet, L. Cassayre, P. Chamelot, J. Finne, D. Noël, P. Taxi, Electrochemical study of the corrosion of metals in molten fluorides, Mater. Sci. Forum 595–598 (2008) 483–490.
[26] R.B. Evans III, J.H. Devan, G.M. Watson, Self-diffusion of Chromium in Nickel-base Alloys, ORNL-2982, (1961).
[27] V. Ignatiev, A. Surenkov, 5.10 – material performance in molten salts, in: Rudy J.M. Konings (Ed.), Comprehensive Nuclear Materials, Elsevier, Oxford, 2012, pp. 221–250.
[28] J.W. Koger, Evaluation of Hastelloy N Alloys After Nine Years Exposure to Both a Molten Fluorided Salt and Air at Temperatures from 700 to 560°C, ORNL-TM-4189, (1972).
[29] HSC Chemistry is a Commercial Software Including a Thermochemicaldatabase, Developed and Sold by Outukumpu, Finland, (2018) (See www.outotec.com/hsc for more details).
[30] C.S. Ni, L.Y. Lu, C.L. Zeng, Y. Niu, Electrochemical impedance studies of the initial-stage corrosion of 310S stainless steel beneath thin film of molten $(0.62Li, 0.38K)_2CO_3$ at 650°C, Corros. Sci. 53 (2011) 1018–1024.